Impact of metal on the DNA photocleavage activity and cytotoxicity of ferrocenyl terpyridine 3d metal complexes

ARTICLE *in* DALTON TRANSACTIONS · NOVEMBER 2011

Impact Factor: 4.2 · DOI: 10.1039/c1dt11102g · Source: PubMed

Dalton Transactions

Cite this: *Dalton Trans.*, 2011, **40**, 11904

www.rsc.org/dalton

PAPER

Impact of metal on the DNA photocleavage activity and cytotoxicity of ferrocenyl terpyridine 3d metal complexes†

Basudev Maity,[a] Sudarshan Gadadhar,[b] Tridib K. Goswami,[a] Anjali A. Karande*[b] and Akhil R. Chakravarty*[a]

Received 12th June 2011, Accepted 22nd August 2011
DOI: 10.1039/c1dt11102g

Ferrocenyl terpyridine 3d metal complexes and their analogues, *viz*. $[M(Fc\text{-}tpy)_2](ClO_4)_2$ (**1–4**), $[Zn(Ph\text{-}tpy)_2](ClO_4)_2$ (**5**) and $[Zn(Fc\text{-}dpa)_2]X_2$ (X = ClO_4, **6**; PF_6, **6a**), where M = Fe(II) in **1**, Co(II) in **2**, Cu(II) in **3** and Zn(II) in **4**, Fc-tpy is 4′-ferrocenyl-2,2′:6′,2″-terpyridine, Ph-tpy is 4′-phenyl-2,2′:6′,2″-terpyridine and Fc-dpa is ferrocenyl-*N*,*N*-dipicolylmethanamine, are prepared and their DNA binding and photocleavage activity in visible light studied. Complexes **2**, **4**, **5** and **6a** that are structurally characterized by X-ray crystallography show distorted octahedral geometry with the terpyridyl ligands binding to the metal in a meridional fashion, with Fc-dpa in **6a** showing a facial binding mode. The Fc-tpy complexes display a charge transfer band in the visible region. The ferrocenyl (Fc) complexes show a quasi-reversible Fc^+-Fc redox couple within 0.48 to 0.66 V *vs.* SCE in DMF-0.1 M TBAP. The DNA binding constants of the complexes are ~10^4 M^{-1}. Thermal denaturation and viscometric data suggest DNA surface binding through electrostatic interaction by the positively charged complexes. Barring the Cu(II) complex **3**, the complexes do not show any chemical nuclease activity in the presence of glutathione. Complexes **1–4** exhibit significant plasmid DNA photocleavage activity in visible light *via* a photoredox pathway. Complex **5**, without the Fc moiety, does not show any DNA photocleavage activity. The Zn(II) complex **4** shows a significant PDT effect in HeLa cancer cells giving an IC_{50} value of 7.5 μM in visible light, while being less toxic in the dark (IC_{50} = 49 μM).

Introduction

Transition metal complexes have been extensively used for biological applications following the success of cisplatin as a chemotherapeutic agent for a variety of cancer cells.[1–10] The inherent dark toxicity and cellular resistivity of cisplatin and its analogues have led to the development of a new generation of platinum-based anticancer agents.[11–15] The use of metal-based photochemotherapeutic agents in photodynamic therapy (PDT) circumvents this problem.[15] A drug in PDT is a photosensitizer which is selectively photoactivated in the cancer cells using visible light leaving the healthy cells unaffected.[16–19] Using the PDT approach, Sadler and coworkers showed that a six-coordinate platinum(IV) complex as a photoactive metallodrug with two *trans*-azide ligands is stable in the dark but forms a diguanidine platinum(II) adduct on photoactivation, killing human cancer cells.[15]

The currently used FDA approved PDT drug is Photofrin® which is an oligomeric mixture of hematoporphyrin.[16] The interest in metal-based PDT agents arises due to the skin toxicity and hepatotoxicity of the porphyrin based drug.[20,21] Besides, the efficacy of an organic photosensitizer in PDT depends primarily on its ability to produce singlet oxygen ($^1O_2$) as the reactive oxygen species (ROS) *via* a type-II pathway.[22,23] Transition metal complexes with versatile coordination geometry, spectral and redox properties could show a similar PDT effect *via* an alternate photoredox or type-I pathway to produce $^{\bullet}OH$ or $O_2^{\bullet-}$ as ROS to damage the cancer cells. Several transition metal complexes are known to exhibit significant photocytotoxicity in visible light in various cancer cells.[5–10,24–30]

The present work aims to develop new ferrocene-conjugated metal complexes that are capable of showing photoinduced cytotoxicity and/or DNA damaging activity for potential application in PDT. The ferrocene molecule as such is stable in biological media with low cytotoxicity, good lipophilicity and unique redox properties.[31] The medicinal importance of the ferrocenyl moiety is evidenced from its activity on incorporation into the antimalarial drug chloroquine or the breast cancer drug tamoxifen.[32,33] The activity and selectivity of these drugs are significantly enhanced in their ferrocenyl conjugates. The oxidized form of ferrocene, *viz*. ferrocenium ion, is also known to be cytotoxic and the anticancer activity of various ferrocene-conjugates are reported.[34–36]

[a]*Department of Inorganic and Physical Chemistry, Indian Institute of Science, Bangalore, 560 012, India. E-mail: arc@ipc.iisc.ernet.in; Fax: 91-80-23600683; Tel: 91-80-22932533*
[b]*Department of Biochemistry, Indian Institute of Science, Bangalore, 560 012, India. E-mail: anjali@biochem.iisc.ernet.in; Tel: 91-80-22932306*

† Electronic supplementary information (ESI) available: Experimental details on DNA binding and cleavage, figures of spectral, voltammetric, DNA binding and cleavage, cytotoxicity and FACScan analysis (Fig. S1–S25). CCDC reference numbers 829878–829881. For ESI and crystallographic data in CIF or other electronic format see DOI: 10.1039/c1dt11102g

Our recent work has shown that ferrocene-conjugated terpyridine copper(II) complexes are efficient DNA photocleavers in red light and exhibit significant photocytotoxicity in visible light.[37] The major predicament is that the redox active copper(II) complexes generally show undesirable dark cytotoxicity in the presence of cellular thiols.[38,39] To explore the impact of the 3d metal in the ferrocenylterpyridine (Fc-tpy) complexes, we have prepared and studied the DNA photocleavage and photocytotoxic properties of ferrocene-conjugated terpyridyl Fe(II), Co(II), Cu(II) and Zn(II) complexes. To understand the effect of the Fc and tpy moieties in Fc-tpy, we have prepared Ph-tpy and Fc-dpa complexes of Zn(II). Herein, we present the synthesis, crystal structure, DNA binding, DNA photocleavage and photocytotoxicity of $[M(Fc\text{-}tpy)_2](ClO_4)_2$ (**1–4**), $[Zn(Ph\text{-}tpy)_2](ClO_4)_2$ (**5**) and $[Zn(Fc\text{-}dpa)_2]X_2$ (X = ClO_4, **6**; PF_6, **6a**), where M = Fe(II) in **1**, Co(II) in **2**, Cu(II) in **3** and Zn(II) in **4**, Fc-tpy is 4′-ferrocenyl-2,2′:6′,2″-terpyridine, Ph-tpy is 4′-phenyl-2,2′:6′,2″-terpyridine and Fc-dpa is ferrocenyl-*N*,*N*-dipicolylmethanamine (Scheme 1). Complex **5** is used as a control species. Complexes **2**, **4**, **5** and **6a** are structurally characterized by X-ray crystallography. The significant results include the photoinduced DNA cleavage activity of **1–4** in red light and the zinc(II) complex **4** showing a remarkable PDT effect in visible light with high photocytotoxicity in HeLa cells but less dark toxicity.

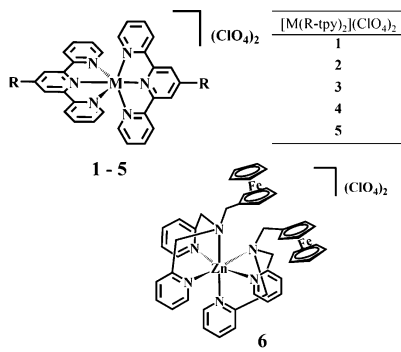

$[M(R\text{-}tpy)_2](ClO_4)_2$	M	R
1	Fe	Ferrocenyl
2	Co	Ferrocenyl
3	Cu	Ferrocenyl
4	Zn	Ferrocenyl
5	Zn	Phenyl

Scheme 1 Complexes **1–6** and the ligands used.

Results and discussion

Synthesis and general properties

Complexes **1–6** are prepared in good yield by reacting the tridentate ligand with the respective metal salt in a 2 : 1 molar ratio in ethanol. The complexes are isolated as perchlorate salts and characterized from spectral and analytical data. Selected physicochemical data are given in Table 1. The complexes essentially show the molecular ion peaks in MeCN corresponding to the $[ML_2]^{2+}$ formulation, where M is the 3d metal ion and L is the tridentate ligand Fc-tpy, Ph-tpy or Fc-dpa indicating the stability of the complexes in a solution phase (Fig. S1–S6, ESI†). The characterization data for **1** and **4** as perchlorate salts compare well with their reported PF_6 analogues.[40] The IR spectra of the complexes show the characteristic ClO_4^- stretch at ~1085 cm^{-1} (Fig. S7, ESI†). The complexes are 1 : 2 electrolytic as evidenced from their molar conductivity data in DMF at 25 °C. While the Fe(II) and Zn(II) complexes are diamagnetic giving characteristic ^1H NMR spectra according to the binary structure of the complexes, the Co(II) and Cu(II) complexes are paramagnetic with three and one unpaired electron, respectively (Fig. S8–S11, ESI†). The absorption spectra of the complexes are recorded in 50% aqueous DMF. The ferrocenyl terpyridine moiety in **1–4** shows a charge transfer band near 540 nm (Fig. 1, Fig. S12, ESI†).[40,41] The Fc-tpy, upon coordination to the 3d metal, lowers the energy of the π_{tpy}^* orbital thus giving this low energy band.

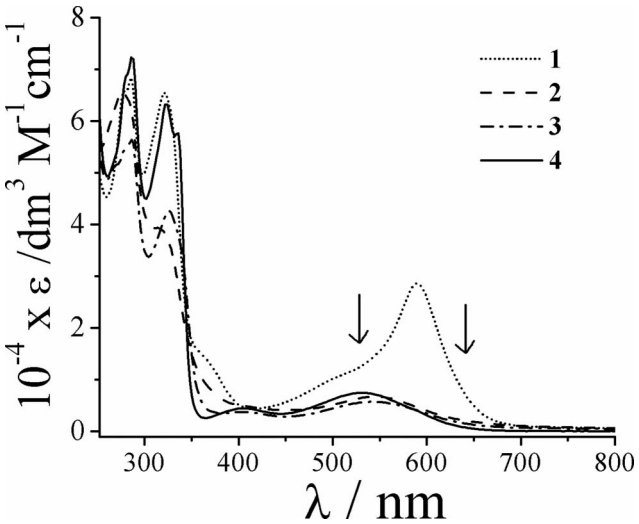

Fig. 1 Electronic absorption spectra of the complexes **1–4** in 50% aqueous DMF. The arrows indicate the wavelengths of laser light used for photo-induced DNA cleavage studies.

Table 1 Selected physicochemical data for the complexes **1–6**

	Cyclic voltammetry: E_f / V (ΔE_p / mV)[a]					IR / cm^{-1} [ν (ClO_4^-)]	λ_{max} / nm (ε / dm^3 M^{-1} cm^{-1})[b]
	Fc^+-Fc	Fe(III)-Fe(II)	Co(III)-Co(II), Co(II)-Co(I)	Cu(II)-Cu(I)	Ligand reductions		
1	0.60 (110)	1.14	—	—	−1.32 (175)	1081	590 (28 520), 515sh (10 500)
2	0.66 (130)	—	0.15 (115), −0.82 (75)	—	−1.64 (85)	1091	543 (6770), 407sh (4704)
3	0.62 (105)	—	—	−0.33(115)	−1.29, −1.36 (140)	1080	542 (5800), 406 (3330)
4	0.62 (100)	—	—	—	−1.30 (75), −1.43 (90)	1086	531 (7550), 406 (3680)
5	—	—	—	—	−1.20 (80), −1.32 (95)	1084	430 (140)
6	0.48 (144)[c]	—	—	—	—	1082	429 (280)

[a] In DMF-0.1 M TBAP. $E_f = 0.5(E_{pa} + E_{pc})$, $\Delta E_p = (E_{pa} - E_{pc})$, where E_{pa} and E_{pc} are the anodic and cathodic peak potential, respectively. The potentials are *vs.* SCE. Scan rate = 50 mV s^{-1}. Fc = $\{(\eta^5\text{-}C_5H_5)Fe(\eta^5\text{-}C_5H_4)\}$. [b] In aq. DMF. sh, shoulder. [c] DPV data showed that this cyclic voltammetric response is a combination of two responses at 0.50 V and 0.45 V *vs.* SCE.

The Fc-tpy complex **1**, with Fe(II) as the 3d metal ion, shows an intense absorption band at 590 nm assignable to the MLCT (metal-to-ligand charge transfer) transition.[40] The Ph-tpy complex **5** does not display a similar spectral band in the absence of the ferrocenyl group. Complex **6** having the Fc-dpa bound to Zn(II) displays only the ferrocene-centred band at 430 nm. The intense ligand centred π–π* transitions in **1–6** are observed in the UV region.

The redox activity of the complexes (**1–6**) has been studied in DMF-0.1 M tetrabutylammonium perchlorate (TBAP) (Table 1). The Fc-tpy complexes show the Fc^+-Fc redox couple at ~0.60 V *vs.* SCE (saturated calomel electrode) (Fig. 2). A significant shift of the anodic potential observed in these complexes in comparison to free ferrocene (0.42 V) indicates stabilization of the Fc moiety towards oxidation in the presence of the electron withdrawing terpyridyl moiety. Complex **6**, where the Fc-dpa ligand binds facially to the Zn(II) centre, shows only a minor shift of the Fc^+-Fc redox couple appearing at 0.48 V in this complex (Fig. 2). Observation of a single DPV (differential pulse voltammetry) peak in complexes **1–3** suggests that the two ferrocenyl moieties are chemically equivalent (Fig. S13, ESI†). DPV of complex **4**, however, shows two close peaks indicating the ferrocenyl moieties in this complex are nearly equivalent. DPV of the Fc-dpa zinc(II) complex **6** shows two oxidation peaks at 0.50 V and 0.45 V *vs.* SCE suggesting structural differences between the Fc-tpy and Fc-dpa complexes (Fig. S13, ESI†).

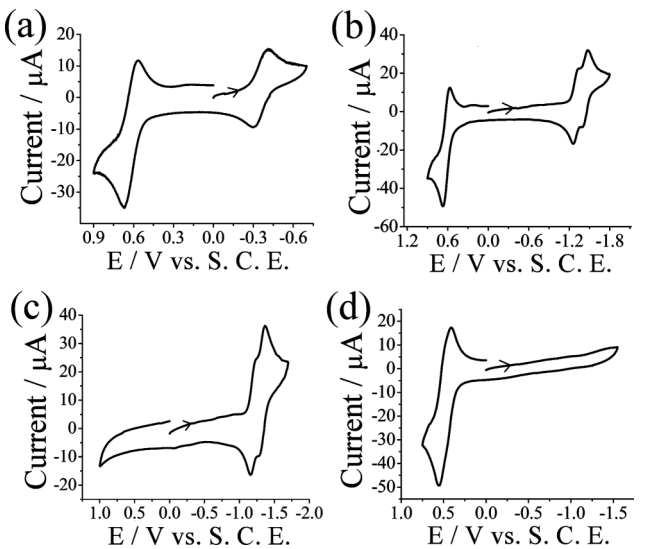

Fig. 2 Cyclic voltammograms of the complexes $[Cu(Fc\text{-}tpy)_2](ClO_4)_2$ (a), $[Zn(Fc\text{-}tpy)_2](ClO_4)_2$ (b), $[Zn(Ph\text{-}tpy)_2](ClO_4)_2$ (c) and $[Zn(Fc\text{-}dpa)_2](ClO_4)_2$ (d) in DMF-0.1 M TBAP at a scan rate of 50 mV s^{-1}.

Complex **1** shows an irreversible Fe(II) to Fe(III) oxidative response at 1.14 V. It also shows a quasireversible cyclic voltammetric ligand reduction at –1.32 V which is a combination of two reduction peaks at –1.28 V and –1.36 V as evidenced from the DPV results (Fig. S14, ESI†). The binary cobalt(II) complex **2** exhibits quasireversible Co(II) to Co(III) oxidation and Co(II) to Co(I) reduction at 0.15 and –0.82 V, respectively. The complex shows only one ligand reduction peak at –1.64 V. The Cu(II)-Cu(I) redox couple in complex **3** is observed at –0.33 V indicating the stabilization of the +2 oxidation state of copper in a CuN_6 core. The ligand reduction is observed at –1.29 V and –1.36 V (Fig. S14, ESI†). Complex **5** without any ferrocenyl moiety shows two quasireversible ligand reductions at –1.20 V and –1.32 V. The ligand reduction for the zinc complex **4** appears at –1.30 V and –1.43 V. The cathodic shift of the ligand reduction potentials in **4** compared to **5** indicates significant interaction between the terpyridyl moiety and ferrocene. Complex **6** does not show any ligand reduction in this potential range.

X-ray crystallography

Complexes **2** as **2**·MeOH·MeCN, **4** as **4**·2MeCN, **5** and **6** as its PF_6 salt **6a** are structurally characterized by single crystal X-ray crystallography. Complexes **2** and **4** crystallize in the $C2/c$ space group of the monoclinic crystal system with four molecules in the unit cell. The complexes are structurally similar. Complexes **5** and **6a** crystallize in monoclinic $P2_1/c$ and orthorhombic $Pbcn$ space groups, respectively. The crystal structures of **2**, **4** and **5** show that the terpyridine moiety binds to the metal centre in a meridional fashion, while Fc-dpa in complex **6a** binds to Zn(II) in a facial mode.[42] The coordination geometry in the structures is distorted octahedral with a MN_6 core. The perspective views of the molecules are shown in Fig. 3–5 (Fig. S15–S19, ESI†). Selected bonding parameters are given in Table 2.

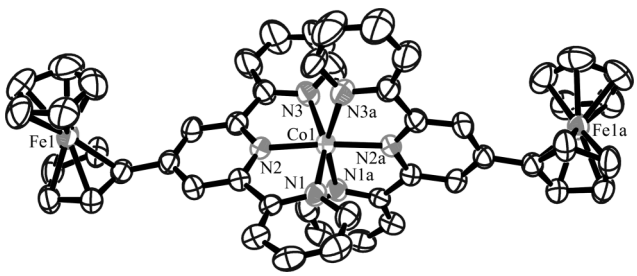

Fig. 3 An ORTEP view of the cationic complex in **2**·MeOH·MeCN showing 50% probability thermal ellipsoids and the atom numbering scheme for the metal and heteroatoms. The hydrogen atoms are not shown for clarity.

The M–N bond distances in the binary terpyridine complexes involving the central pyridyl ring of Fc-tpy or Ph-tpy are shorter (1.945 to 2.069 Å) compared to other M–N distances (2.093 to

Table 2 Selected bond distances[a] (Å) for the complexes **2**·MeOH·MeCN, **4**·2MeCN, **5** and **6a**

	2	**4**	**5**	**6a**
M(1)–N(1)	2.105(4)	2.164(6)	2.192(4)	2.180(4)
M(1)–N(2)	1.945(4)	2.062(5)	2.069(4)	2.318(4)
M(1)–N(3)	2.093(5)	2.211(6)	2.193(4)	2.118(4)
M(1)–N(4)	—	—	2.178(4)	—
M(1)–N(5)	—	—	2.091(4)	—
M(1)–N(6)	—	—	2.217(4)	—
Fe(1)–C_0^1	1.636	1.641	—	1.657
Fe(1)–C_0^2	1.643	1.644	—	1.639

[a] M(1) = Co(1) in **2** and Zn(1) in **4**, **5** and **6a**. The C_0^1 and C_0^2 are two centroids of the cyclopentadienyl rings comprising of atoms C(1) to C(5) and C(6) to C(10), respectively. The Fe(1)–C distances are in the range of 2.015(6) to 2.049(6) Å for **2**, 2.038(10) to 2.079(11) Å for **4** and 1.993(8) to 2.055(8) Å for **6a**. The average Fe(1)–C distances are 2.032(6) Å, 2.038(10) Å and 2.026(7) Å for **2**, **4** and **6a**, respectively.

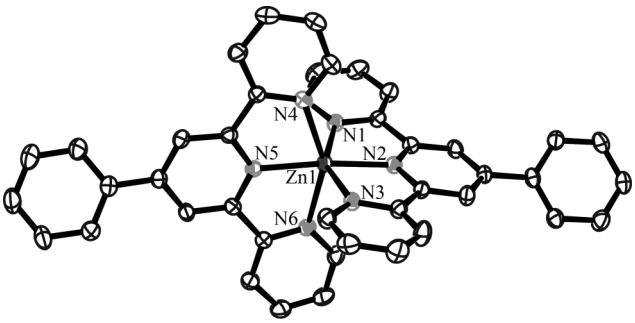

Fig. 4 An ORTEP view of the cationic complex in **5** showing 50% probability thermal ellipsoids and the atom numbering scheme for the metal and heteroatoms. The hydrogen atoms are not shown for clarity.

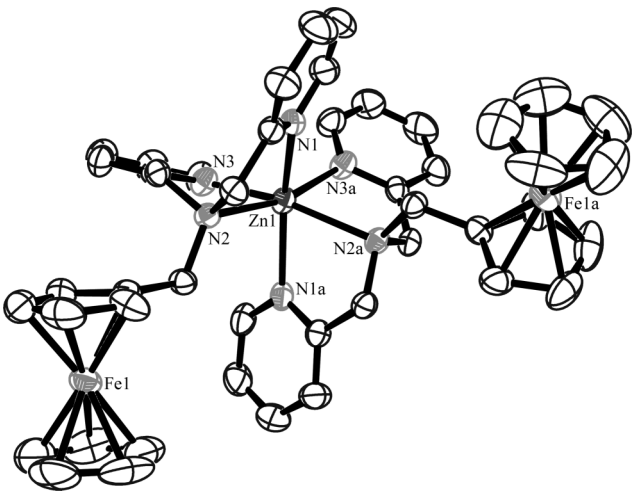

Fig. 5 An ORTEP view of the cationic complex in **6a** showing 50% probability thermal ellipsoids and the atom numbering scheme for the metal and heteroatoms. The hydrogen atoms are not shown for clarity.

2.193 Å) involving the terminal pyridyl groups.[43,44] In complex **6a**, the bond distance between zinc and the amine nitrogen is longer (2.318 Å) than with the terminal pyridyl groups (2.118 and 2.180 Å) indicating flexibility of the Fc-dpa ligand. The cyclopentadienyl (Cp) rings of the ferrocenyl moiety in **2**, **4** and **6a** are essentially in an eclipsed conformation. The dihedral angles between the Cp rings of the ferrocenyl moiety in these structures are ~2–3° indicating their parallel orientation. The phenyl rings of two Ph-tpy ligands in complex **5** are nearly parallel making a dihedral angle of 6.67°. The dihedral angle between the phenyl groups with the central pyridyl rings in Ph-tpy ligands containing N2 and N5 atoms are 44.30° and 32.29°, respectively, while the same angles between the Cp ring and the central pyridine ring in complexes **2** and **4** are 8.78° and 10.08°, respectively.

DNA binding study

The ability of the complexes to interact with double stranded calf thymus DNA has been examined by performing UV-visible absorption titration, thermal denaturation and viscometric titration experiments. Selected DNA binding data are listed in Table 3. In the absorption titration method, the binding affinity of the complexes is quantified by determining the intrinsic equilibrium binding constant (K_b) values.[45] Addition of DNA to the complex

Table 3 Selected DNA binding parameters for the complexes **1–6**

Complex	K_b[a] / M^{-1}	s[b]	ΔT_m[c]
1	$(8.3 \pm 0.2) \times 10^4$	0.02	0.4
2	$(4.7 \pm 0.6) \times 10^4$	0.03	0.9
3	$(6.8 \pm 0.7) \times 10^4$	0.06	0.2
4	$(1.1 \pm 0.3) \times 10^4$	0.02	0.6
5	$(1.0 \pm 0.4) \times 10^5$	0.1	2.4
6	—		0.1
EB[d]	—		11.2

[a] Intrinsic equilibrium DNA binding constant and fitting parameter values are from UV-visible titration experiments. [b] McVH equation fitting parameter. [c] Change in the calf thymus DNA melting temperature. [d] EB = ethidium bromide.

solution (15–25 μM) in Tris-HCl buffer medium (pH 7.2) shows a moderate hypochromicity (~5–20%) at 318 nm (Fig. 6, Fig. S20, ESI†). The K_b values of the complexes are within $(1.1 \pm 0.3) \times 10^4$ to $(1.0 \pm 0.4) \times 10^5$ M^{-1}. The reduced binding strength compared to the DNA intercalator ethidium bromide is possibly due to the absence of any planar DNA binding moiety in these complexes. The K_b value of **6** could not be determined due to no apparent hypochromicity observed for this complex.

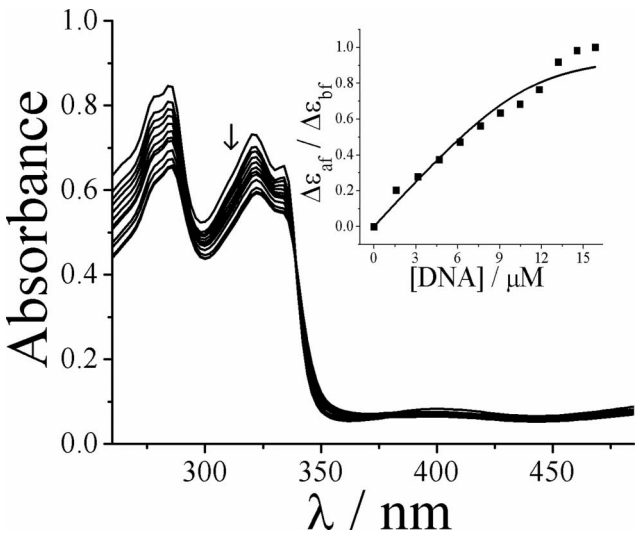

Fig. 6 Spectral traces showing the effect of gradual addition of CT DNA (150 μM NP) to the 15 μM solution of $[Zn(Fc\text{-}tpy)_2](ClO_4)_2$ (**4**) in DMF-Tris-HCl buffer medium. The inset shows the plot of $\Delta\varepsilon_{af}/\Delta\varepsilon_{bf}$ *vs.* [DNA].

Thermal denaturation experiments are carried out to study the stability of the duplex calf thymus DNA in the presence of the complexes **1–6**. The unwinding of duplex DNA to single stranded DNA at the melting temperature is known to cause a significant increase in the absorption intensity at 260 nm.[46] The stabilization of duplex DNA by an external molecule causes an increase in its melting temperature. DNA intercalators give high DNA melting temperatures compared to the surface/groove binding molecules. The present complexes show only a minor increase in the melting temperature (0.1–2.4 °C) indicating moderate stabilization of the double helical structure of DNA on binding to these complexes (Fig. 7(a), Fig. S21(a), ESI†). The ΔT_m value for the DNA intercalator ethidium bromide under similar experimental

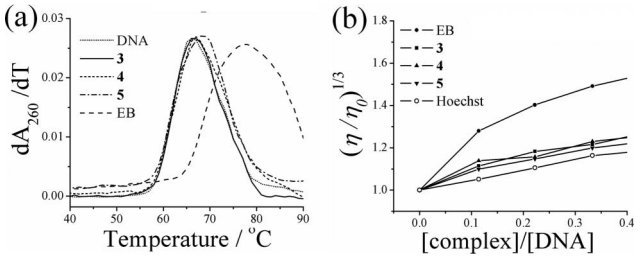

Fig. 7 (a) DNA melting plots for the CT DNA (150 μM NP) alone and in the presence of complexes **3–5** (15 μM) and ethidium bromide (EB, 15 μM) in 5 mM phosphate buffer (pH = 6.8). (b) The effect of addition of increasing amounts of complexes **3–5**, EB and Hoechst 33258 on the relative viscosity of CT DNA at 37.0 (±0.1) °C in 5 mM Tris-HCl buffer (pH = 7.2).

conditions is 11.2 °C. The DNA melting data suggest a surface and/or electrostatic binding nature of the binary complexes.

The viscometric titration method has been used to study the nature of DNA binding of the complexes. The specific viscosity of the DNA duplex is closely related to its contour length.[47] Intercalator molecules like ethidium bromide cause a significant increase in the DNA contour length compared to the groove binding molecules. The intercalator molecules thus have a large effect on the change in the relative specific viscosity whereas the surface or groove binding molecules have no significant effect. The effect of increasing concentration of the complexes **1–6** on the relative specific viscosity $(\eta/\eta_0)^{1/3}$ of the DNA solution is shown in Fig. 7(b) (Fig. S21(b), ESI†), where η and η_0 are the specific viscosity of DNA in the presence and absence of the complex, respectively. A comparison of the viscosity data along with those of the DNA intercalator ethidium bromide and DNA groove binder Hoechst 33258 suggests a surface and/or electrostatic binding nature of the binary complexes.

Chemical nuclease activity

Oxidative cleavage of supercoiled (SC) pUC19 DNA (0.2 μg, 30 μM) by the complexes **1–6** has been studied using glutathione as a reducing agent and hydrogen peroxide as an oxidizing agent (Fig. 8). The Cu(II) complex **3** shows chemical nuclease activity, while other complexes do not show any apparent DNA cleavage activity with glutathione. This is due to the presence of a Cu(II)-Cu(I) redox couple at –0.33 V *vs.* SCE. Complexes **1** and **6** show moderate DNA cleavage activity in the presence of hydrogen peroxide. The Fe(II) complex **1** could be involved in a Fenton-type reaction in the presence of H_2O_2.[48] The lower oxidation potential of the ferrocenyl moiety in complex **6** could make it chemical nuclease active in the presence of H_2O_2. Control experiments show that GSH and H_2O_2 alone do not show any significant cleavage of SC DNA.

DNA photocleavage activity

The ability of the complexes **1–6** to cleave SC pUC19 DNA has been examined in the presence of green light of 532 nm and red light of 647 nm in 50 mM Tris-HCl/NaCl buffer (pH 7.2) (Fig. 9, Fig. S22, ESI†). The choice of these wavelengths is based on the visible absorption bands observed for the Fc-tpy complexes **1–4**. The Fe(II) complex **1** shows significant DNA

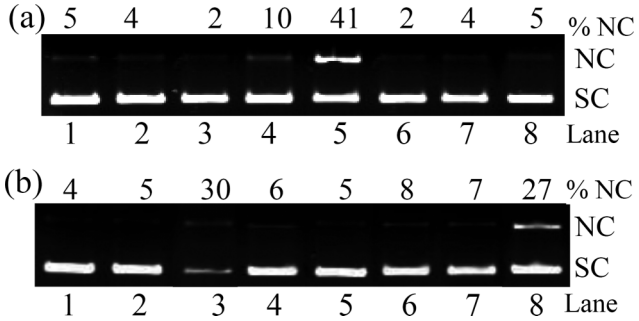

Fig. 8 Gel electrophoresis diagram showing the chemical nuclease activity of complexes **1–6** (20 μM) using SC pUC19 DNA (0.2 μg, 30 μM b.p.) in the presence of 1 mM glutathione (GSH) as a reducing and 0.20 mM H_2O_2 as an oxidizing agent: (a) lane-1, DNA control; lane-2, DNA + GSH; lane-3, DNA + **1** + GSH; lane-4, DNA + **2** + GSH; lane-5, DNA + **3** + GSH; lane-6, DNA + **4** + GSH; lane-7, DNA + **5** + GSH; lane-8, DNA + **6** + GSH and (b) lane-1, DNA control; lane-2, DNA + H_2O_2; lane-3, DNA + **1** + H_2O_2; lane-4, DNA + **2** + H_2O_2; lane-5, DNA + **3** + H_2O_2; lane-6, DNA + **4** + H_2O_2; lane-7, DNA + **5** + H_2O_2; lane-8, DNA + **6** +H_2O_2.

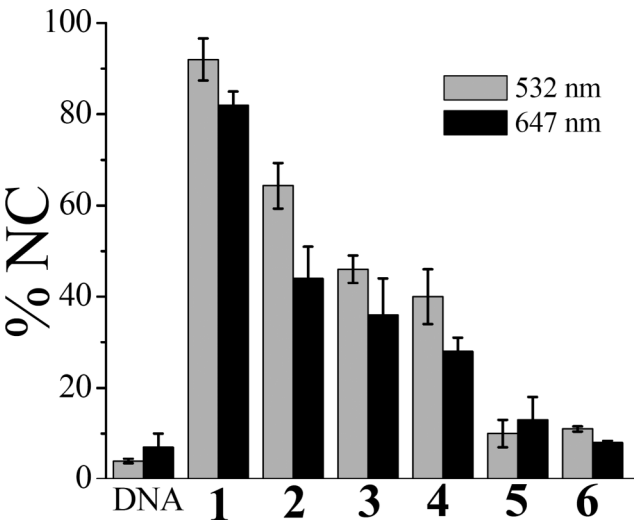

Fig. 9 Bar diagram showing the visible light-induced pUC19 DNA (0.2 μg, 30 μM b.p.) photocleavage activity of the complexes **1–6** (20 μM) in green light of 532 nm (gray shade) and red light of 647 nm (black shade) for an exposure time of 1.0 h.

cleavage activity (~90% NC DNA) in green as well as red light, whereas complexes **2–4** show only moderate DNA photocleavage activity. Binary Zn(II) complexes of the Ph-tpy and Fc-dpa ligands do not show any significant DNA photocleavage activity. The DNA photocleavage activity in visible light follows the order: **1** [Fc-tpy/Fe(II)] >> **2** [Fc-tpy/Co(II)] > **3** [Fc-tpy/Cu(II)] ≥ **4** [Fc-tpy/Zn(II)] >> **5** [Ph-tpy/Zn(II)] ~ **6** [Fc-tpa/Zn(II)]. The DNA photocleavage activity of the Fe(II) complex could be due to the high absorption coefficient value (ε = 28 520 dm^3 M^{-1} cm^{-1}) of its visible spectral band at 590 nm when compared to other metal complexes having an ε value of ~6000 dm^3 M^{-1} cm^{-1}. The inactivity of the Zn(II) complex **5** and moderate activity of complex **4** suggest the important role of the Fc-tpy ligand in the DNA photocleavage reaction. The presence of redox active metals, *viz*. Fe(II), Co(II) and Cu(II), makes the complexes more active than the redox inactive Zn(II) complex. The ferrocenyl Zn(II) complex **6** does not show any apparent DNA cleavage activity in the absence of the photoactive

terpyridyl moiety. The Fc-tpy and Ph-tpy ligands alone do not show any DNA cleavage activity. The complexes are inactive in the dark thus ruling out any possibility of hydrolytic cleavage of DNA.[49]

To explore the mechanistic aspects of the reactions, control experiments have been carried out using complex **3** in the presence of various additives including sodium azide (NaN_3) and tetramethylpiperidone (TEMP) as singlet oxygen quenchers, dimethyl sulfoxide (DMSO), potassium iodide (KI) and catalase as hydroxyl radical scavengers and superoxide dismutase (SOD) as a superoxide scavenger (Fig. 10). Hydroxyl radical scavengers show significant inhibition of DNA photocleavage activity indicating the formation of hydroxyl radical (˙OH) species. The ˙OH radical is possibly generated *via* the superoxide radical as evidenced from complete inhibition of the DNA cleavage activity in the presence of SOD. The superoxide radical in aqueous medium could generate reactive ˙OH species. The $^1O_2$ quenchers do not show any apparent inhibition in the DNA photocleavage activity thus ruling out the type-II energy transfer pathway.[22,23] Formation of ˙OH/superoxide anion radical could take place *via* a photoredox pathway. The DNA groove binding propensity of the complexes has been studied using complex **3** and a DNA minor groove binder distamycin-A.[50] Inhibition of DNA cleavage by **3** in the presence of distamycin-A suggests surface binding of the binary complexes at the minor groove (Fig. 10, lane 9).

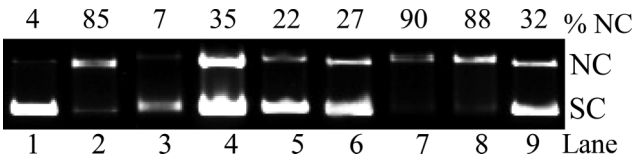

Fig. 10 Gel electrophoresis diagram showing the visible light-induced DNA cleavage activity of $[Cu(Fc\text{-}tpy)_2](ClO_4)_2$ (**3**, 30 μM) at 532 nm using SC pUC19 DNA (0.2 μg, 30 μM b.p.) for an exposure time of 1 h in the presence of additives: lane-1, DNA control; lane-2, DNA + **3**; lane-3, DNA + SOD (15 units) + **3**; lane-4, DNA + DMSO (8 μL) + **3**; lane-5, DNA + KI (5 mM) + **3**; lane-6, DNA + catalase (10 units) + **3**; lane-7, DNA + NaN_3 (5 mM) + **3**; lane-8, DNA + TEMP (5 mM) + **3**; lane-9, DNA + distamycin-A (0.4 mM) + **3**.

We have performed photolysis experiments using complexes **3** and **4**. The complexes in aqueous DMF show charge transfer bands at 531 and 542 nm. Irradiation of the complexes in UV-A light of 365 nm shows the appearance of a new absorption band at ~578 nm, while no such change is observed on keeping the solution in the dark (Fig. S23, ESI†). A similar absorption band appears upon addition of an oxidizing agent such as aqueous ammonium cerium(IV) nitrate to the solution of the complexes, indicating the susceptibility of the ferrocenyl moiety towards photooxidation. An acetonitrile solution of complex **4** on exposure to UV-A light of 365 nm for 1 h does not show any peak at ~578 nm. However, an aqueous MeCN solution of the complex exhibits a similar effect to that observed in aqueous DMF. The results indicate that the photo-oxidation of the ferrocenyl moiety occurs only in an aqueous solvent. The oxidized form of ferrocene is known to degrade in an aqueous medium to generate reactive hydroxyl radicals.[34]

Photocytotoxic property

The cytotoxicity of complexes **1–6** in HeLa cells has been studied in the dark and in visible light (400–700 nm, 1 h photoexposure). The IC_{50} values are obtained from the MTT (3-(4,5-dimethyl-2-thiazolyl)-2,5-diphenyl-2*H*-tetrazolium bromide) assay (Fig. 11, Fig. S24, ESI†). The Fc-tpy complex of Cu(II) (**3**) is cytotoxic in the dark giving an IC_{50} value of 6.7 μM. High cytotoxicity of the Cu(II) complex could be due to its chemical nuclease activity in the dark in the presence of reducing cellular thiols like GSH. Complex **3** shows only a moderate increase in cytotoxicity on exposure to light giving an IC_{50} value of 3.1 μM. Complex **3** having the ferrocenyl moiety is significantly photocytotoxic compared to the copper(II) complex of the Ph-tpy ligand, *viz*. $[Cu(Ph\text{-}tpy)_2](NO_3)_2$, which gives an IC_{50} value of 24.1 μM in visible light.[51] Complex **4** having a redox inactive Zn(II) centre is less cytotoxic in the dark (IC_{50} = 49.1 μM) than its Cu(II) analogue. Complex **4**, however, shows significant photocytotoxicity in the light giving an IC_{50} value of 7.5 μM. The Ph-tpy complex **5** does not show any apparent cytotoxicity in this concentration range. The Fc-tpy moiety thus plays an important role in the photocytotoxic behavior of complex **4** in HeLa cells. It is intriguing that both the Fe(II) and Co(II) complexes (**1**, **2**) that are found to show significant plasmid DNA photocleavage activity in visible light are not cytotoxic in HeLa cells, giving IC_{50} values of >50 μM in both light and dark conditions within the concentration range used. Complexes **5** and **6** also do not show any cytotoxicity. The IC_{50} values that are listed in Table 4 show the impact of the ferrocenyl ligand and the 3d metal ion on the cytotoxic properties of the complexes. The photocytotoxicity of complex **4** is comparable to that of Photofrin®, with IC_{50} values of 2.57 μM in red light and >25 μM in dark.[52] Cisplatin does not show any PDT effect in HeLa cells giving IC_{50} values of 7.2 and 71.3 μM in the dark after 24 h and 4 h incubation, respectively.[53,54] The photocytotoxic behaviour of complex **4** in comparison to its analogues could be due to the presence of a redox inactive Zn(II) metal centre which remains unaffected by the reducing cellular thiols. We have not made any attempt to explore the composition of the complexes inside the cell on photolysis.

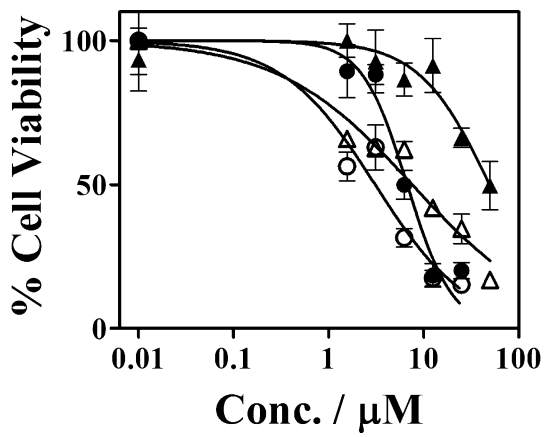

Fig. 11 Cytotoxicity of $[Cu(Fc\text{-}tpy)_2](ClO_4)_2$ (**3**) and $[Zn(Fc\text{-}tpy)_2](ClO_4)_2$ (**4**) in human cervical HeLa cancer cells upon 4 h incubation in the dark followed by photoexposure to visible light (400–700 nm) as determined by MTT assay. The dark-treated and photoexposed cells are shown by (●), (○) symbols for **3** and (▲), (△) symbols for **4**, respectively.

Table 4 A comparison of the IC_{50} values of complexes **1–6**, Photofrin® and cisplatin in HeLa cells

Complex	IC_{50} /μM (visible light)	IC_{50} / μM (dark)
$[Fe(Fc\text{-}tpy)_2](ClO_4)_2$, **1**	>50	>50
$[Co(Fc\text{-}tpy)_2](ClO_4)_2$, **2**	>50	>50
$[Cu(Fc\text{-}tpy)_2](ClO_4)_2$, **3**	3.1 (±0.3)	6.7 (±0.7)
$[Zn(Fc\text{-}tpy)_2](ClO_4)_2$, **4**	7.5 (±0.7)	49.1 (±1.5)
$[Zn(Ph\text{-}tpy)_2](ClO_4)_2$, **5**	>50	>50
$[Zn(Fc\text{-}dpa)_2](ClO_4)_2$, **6**	>50	>50
$[Cu(Fc\text{-}tpy)(dppz)](ClO_4)_2$[a]	3.7	10.5
$[Cu(Ph\text{-}tpy)_2](NO_3)_2$[b]	24.1	24.4
Photofrin®[c]	2.57	>25
Cisplatin[d]	—	7.2[e]

[a] The IC_{50} values are taken from ref. 37 [b] The IC_{50} values are from ref. 51. [c] The IC_{50} values are from ref. 52. [d] Cisplatin IC_{50} value for 24 incubation is from ref. 53. [e] IC_{50} value of cisplatin for 4 h incubation is 71.3 μM (ref. 54).

FACScan analysis for apoptosis

Of the six complexes tested, only complex **4** has shown significant activity with respect to its photocytotoxic properties in the light. To confirm whether the cytotoxic effect is by induction of apoptosis, we have carried out flow cytometric analysis of HeLa cells treated with complex **4**. Cells treated with the complex in the dark are exposed to visible light and then stained with propidium iodide to check for fragmented DNA which is indicated by the increase in the sub-G1/G0 population. It is observed that a concentration of 20 μM complex induced appreciable apoptosis in 24 h and the extent of apoptosis increased on increasing the concentration (Fig. 12, Fig. S25, ESI†). It is also observed that the concentrations used for the experiments induce very low apoptosis in cells incubated in the dark.

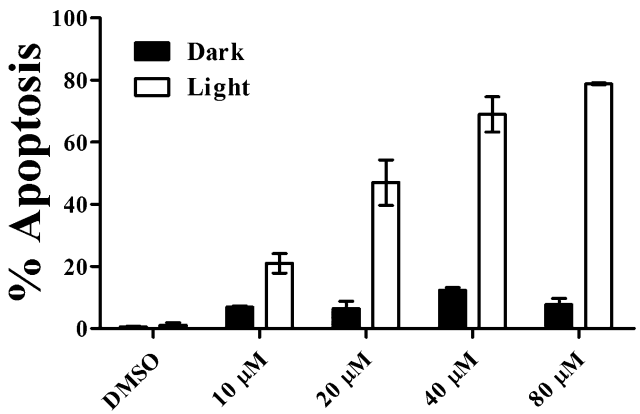

Fig. 12 Bar diagram showing % apoptosis induced in HeLa cells by **4** in the absence or presence of visible light (400–700 nm) obtained from FACScan analysis.

Conclusions

A new class of ferrocene-conjugated Fe(II), Co(II), Cu(II) and Zn(II) complexes are prepared, structurally characterized and their DNA binding and photoinduced DNA cleavage activity in visible light and cytotoxicity in HeLa cells studied. The complexes are redox active and show quasi-reversible cyclic voltammetric responses due to Fc^+-Fc, Cu(II)-Cu(I), Co(III)-Co(II), Co(II)-Co(I) and Fe(III)-Fe(II) couples. The effect of the 3d metal and the ferrocenyl terpyridine moiety is observed from the DNA photocleavage activity of the complexes in visible light. The ferrocenyl group in conjugation with the tpy moiety forms an active moiety to induce significant photocleavage of DNA in visible light. The DNA photocleavage proceeds *via* a photoredox pathway forming hydroxyl radicals. Among the complexes studied, only the Zn(II) complex of the Fc-tpy ligand exhibits a significant PDT effect in HeLa cells in visible light *via* an apoptotic pathway. The results are of importance towards designing new generation ferrocene-based photocytotoxic agents for cellular applications in PDT.

Experimental

Materials

The reagents and chemicals were procured from commercial sources. Ferrocene-2-carboxaldehyde, 2-acetylpyridine, sodium perchlorate, calf thymus DNA, agarose (molecular biology grade), catalase, superoxide dismutase, TEMP (2,2,6,6-tetramethyl-4-piperidone), DABCO (1,4-diazabicyclo [2.2.2] octane) and ethidium bromide were purchased from Sigma-Aldrich (USA). Supercoiled pUC19 DNA (caesium chloride purified) was from Bangalore Genie (India). Tris(hydroxymethyl)aminomethane-HCl (Tris-HCl) buffer (pH 7.2) and phosphate buffer (pH 6.8) were prepared using double distilled water. The solvents were purified by standard procedures.[55] The Fc-tpy, Ph-tpy, Fc-dpa ligands and the binary complexes were prepared by following the literature procedures.[56–59] DMEM, FBS and PI were procured from Sigma Fine Chemicals. Glutamax and Trypsin-EDTA were from Invitrogen.

Measurements

NMR spectra were recorded using a Bruker Avance 400 (400 MHz) NMR spectrometer. Elemental analyses were performed using a Thermo Finnigan FLASH EA 1112 CHNS analyzer. Mass spectra were obtained from a Bruker Esquire 300 plus ESI (Bruker Daltonics) spectrometer. IR spectra of the solid samples were recorded on a PerkinElmer Lamda 35 instrument. Electronic absorption spectral and DNA melting experiments were carried out using a Perkin Elmer Scan-Lambda 650 UV-visible spectrometer. Conductivity measurements were recorded using a Control Dynamics (India) conductivity meter. Cyclic voltammetric measurements were carried out at room temperature on a EG&G PAR 253 VersaStat potentiostat/galvanostat using a three electrode configuration consisting of a glassy carbon working, a platinum wire auxilary and a saturated calomel reference (SCE) electrode. Ferrocene (E_f = 0.42 V) was used as a standard in DMF containing 0.1 M TBAP. Room temperature magnetic susceptibilities of the cobalt(II) complex **2** and copper(II) complex **3** were measured in 1%TMS-DMSO-d_6 solution (v/v). The magnetic moments were calculated by the Evans method using the equation: $\mu_{eff} = 0.0618(\Delta fT/fM)$, where Δf is the observed chemical shift of the TMS signal in Hz, T is the T/K, f is the frequency (MHz) of the NMR spectrometer, and M is the molarity of the complex solution.[60]

Caution! Perchlorate salts of metal complexes are potentially explosive—only small quantities of the samples were handled with great caution and care.

Synthesis

The complexes were prepared by following a general synthetic procedure in which an ethanol suspension of the ligand (2.0 mmol: 0.83 g, Fc-tpy; 0.61 g, Ph-tpy; 0.80 g, Fc-dpa) was reacted with the respective chloride or metal nitrate (1.0 mmol: $FeCl_2{\cdot}4H_2O$, 0.19 g; $Co(NO_3)_2{\cdot}6H_2O$, 0.29 g; $Cu(NO_3)_2{\cdot}3H_2O$, 0.23 g; $Zn(NO_3)_2{\cdot}6H_2O$, 0.29 g) in water with continuous stirring under a nitrogen atmosphere. The resulting solution was refluxed for 15 min followed by cooling to an ambient temperature and stirring was continued for a further period of 1.0 h. The solution was filtered and to the filtrate was added an aqueous solution of sodium perchlorate (2.0 mmol, 0.28 g) and stirred for 15 min. The precipitate thus obtained was collected by filtration, washed with cold ethanol and finally dried in vacuum over P_4O_{10} (Yield: 60–70%).

Anal. Calcd for $C_{50}H_{38}Cl_2Fe_3N_6O_8$ (**1**): C, 55.13; H, 3.52; N, 7.71. Found: C, 54.96; H, 3.31; N, 7.51. FT-IR (KBr phase): 3092 w(br), 1605 s, 1547 w, 1500 m, 1435 m, 1396 m, 1253 w, 1081 vs, 881 m, 829 m, 784 s, 743 m, 621 s, 581 w, 884 m, 445 w cm^{-1} (br, broad; vs, very strong; s, strong; m, medium; w, weak). ESI-MS in MeCN: m/z 445.47 $[M–2ClO_4]^{2+}$. UV-visible in aqueous DMF (1 : 1 v/v) [λ_{max}, nm (ε, $dm^3\ M^{-1}\ cm^{-1}$)]: 590 (28 520), 515 (1050)sh, 360 (14 700)(sh), 329 (60 600)(sh), 320 (65 320), 286 (68 380), 276 (65 600), 271 (56 070) (sh, shoulder). Λ_M, S $m^2\ M^{-1}$ in DMF at 25 °C: 136. ^{1}H-NMR (400 MHz, DMSO-d_6): δ = 9.32 (s, 4H), 9.0 (d, J = 8.0, 4H), 8.03 (m, 4H), 7.23 (d, J = 4.4 Hz, 8H), 5.66 (pst, J = 2.6 Hz, 4H), 4.86 (pst, J = 1.6 Hz, 4H), 4.41 (s, 10H) (s, 10H) (s, singlet; d, doublet; pst, pseudotriplet; m, multiplet).

Anal. Calcd for $C_{50}H_{38}Cl_2CoFe_2N_6O_8$ (**2**): C, 54.57; H, 3.51; N, 7.69. Found: C, 54.39; H, 3.28; N, 7.52. FT-IR (KBr phase): 3096 w, 1609 s, 1542 w, 1496 m, 1460 m, 1433 m, 1250 w, 1091 vs, 1016 s, 876 w, 824 w, 792 s, 745 w, 665 w, 619 s, 578 w, 477 m, 427 w cm^{-1}. ESI-MS in MeCN: m/z 447.07 $[M–2ClO_4]^{2+}$. UV-visible in aqueous DMF (1 : 1 v/v) [λ_{max}, nm (ε, $dm^3\ M^{-1}\ cm^{-1}$)]: 543 (6770), 407 (4704)(sh), 328 (35 150)(sh), 317 (39 140), 284 (63 660), 276 (65 780), 268 (61 990)(sh). Λ_M, S $m^2\ M^{-1}$ in DMF at 25 °C: 134. μ_{eff} = 4.1 μ_B at 298 K.

Anal. Calcd for $C_{50}H_{38}Cl_2CuFe_2N_6O_8$ (**3**): C, 54.74; H, 3.49; N, 7.66. Found: C, 54.43; H, 3.11; N, 7.49. FT-IR (KBr phase): 3100 w(br), 1606 s, 1540 m, 1497 w, 1469 m, 1432 m, 1383 w, 1253 w, 1163 w, 1080 vs, 1013 s, 880 w, 823 m, 792 s, 733 w, 665 w, 613 s, 582 w, 507 m, 473 m cm^{-1}. ESI-MS in MeCN: m/z 449.60 $[M–2ClO_4]^{2+}$. UV-visible in aqueous DMF (50% DMF) [λ_{max}, nm (ε, $dm^3\ M^{-1}\ cm^{-1}$)]: 542 (5800), 406 (3330), 337 (36 430), 328 (35 150)(sh), 326 (4270), 286 (56 300), 279 (54 600), 268 (51 530). Λ_M, S $m^2\ M^{-1}$ in DMF at 25 °C: 134. μ_{eff} = 1.82 μ_B at 298 K.

Anal. Calcd for $C_{50}H_{38}Cl_2Fe_2N_6O_8Zn$ (**4**): C, 54.65; H, 3.49; N, 7.65. Found: C, 54.42; H, 3.22; N, 7.76. FT-IR (KBr phase): 3094 w(br), 1601 s, 1547 m, 1500 w, 1469 m, 1427 m, 1337 w, 1304 w, 1252 w, 1086 vs, 1017 s, 885 m, 831 m, 788 s, 732 m, 673 w, 616 s, 577 w, 505 m, 474 m cm^{-1}. ESI-MS in MeCN: m/z 449.67 $[M–2ClO_4]^{2+}$. UV-visible in aqueous DMF (50% DMF) [λ_{max}, nm (ε, $dm^3\ M^{-1}\ cm^{-1}$)]: 531 (7550), 406 (3680), 336 (56 660)(sh), 323 (62 200), 286 (71 310), 280 (67 590)(sh), 269 (51 540)sh. Λ_M, S $m^2\ M^{-1}$ in DMF at 25 °C:133. ^{1}H-NMR (400 MHz, DMSO-d_6): δ = 9.07 (d, J = 8.0 Hz, 4H), 8.99 (s, 4H), 8.26 (t, J = 4.4 Hz, 4H), 7.9 (d, J = 4.8 Hz, 4H), 7.49 (t, J = 7.2 Hz, 4H), 5.63 (pst, J = 1.6 Hz, 4H), 4.82 (pst, J = 1.8 Hz, 4H), 4.29 (s, 10H) (t, triplet).

Anal. Calcd for $C_{42}H_{30}Cl_2N_6O_8Zn$ (**5**): C, 57.13; H, 3.42; N, 9.52. Found: C, 56.83; H, 3.08; N, 9.62. FT-IR (KBr phase): 3082 w(br), 1604 m, 1550 m, 1469 m, 1412 m, 1245 s, 1165 w, 1084 vs, 1014 s, 972 w, 879 w, 793 m, 767 s, 735 w, 694 m, 650 w, 616 s, 498 w, 413 w cm^{-1}. ESI-MS in MeCN: m/z 341.67 $[M-2ClO_4]^{2+}$. UV-visible in aqueous DMF (50% DMF) [λ_{max}, nm (ε, $dm^3\ M^{-1}\ cm^{-1}$)]: 430 (140), 338 (26 590)(sh), 326 (30 780), 285 (78 000), 280 (76 300)(sh), 269 (62 620)(sh). Λ_M, S $m^2\ M^{-1}$ in DMF at 25 °C: 146. ^{1}H-NMR (400 MHz, DMSO-d_6): δ = 9.38 (s, 4H) 9.14 (d, J = 8.0, 4H), 8.41 (d, J = 7.2 Hz, 4H), 8.26 (t, J = 7.6 Hz, 4H), 7.94 (d, J = 4.4 Hz, 4H), 7.76–7.70 (m, 6H), 7.47 (t, J = 6.2 Hz, 4H).

Anal. Calcd for $C_{46}H_{46}Cl_2Fe_2N_6O_8Zn$ (**6**): C, 52.18; H, 4.38; N, 7.94. Found: C, 52.03; H, 4.53; N, 7.68. FT-IR (KBr phase): 3074 w(br), 2938 w(br), 1607 m, 1573 w, 1447 w, 1435 m, 1367 w, 1336 w, 1310 w, 1237 w, 1157 w, 1082 vs, 1020 s, 932 w, 832 m, 764 s, 619 w, 513 w, 481 w, 477 m, 420 w cm^{-1}. ESI-MS in MeCN: m/z 429.47$[M–2ClO_4]^{2+}$. UV-visible in aqueous DMF (50% DMF) [λ_{max}, nm (ε, $dm^3\ M^{-1}\ cm^{-1}$)]: 429 (280), 261 (31 460). Λ_M, S $m^2\ M^{-1}$ in DMF at 25 °C: 135. ^{1}H-NMR (400 MHz, DMSO-d_6): δ = 8.60 (d, J = 3.6 Hz, 2H), 8.46 (d, J = 4.0, 2H), 8.06 (t, J = 7.2 Hz, 2H), 7.75 (t, J = 7.2 Hz, 2H), 7.62–7.50 (m, 6H), 7.22 (t, J = 6.4 Hz, 2H), 4.38 (s, 2H), 4.30 (s, 2H), 4.20 (s, 2H), 4.90 (s, 7H), 4.01 (s, 5H), 3.61 (s, 8H), 3.53 (s, 2H), 3.46 (s, 2H). Complex **6** was crystallized as its PF_6 salt (**6a**) for structural characterization on adding NH_4PF_6 instead of $NaClO_4$ to the reaction mixture.

Solubility and stability

The complexes were soluble in DMF, DMSO and MeCN. The complexes were stable in aqueous DMF.

X-ray crystallographic procedure

X-ray quality single crystals of the complexes $[Co(Fc\text{-}tpy)_2](ClO_4)_2$ (**2**), $[Zn(Fc\text{-}tpy)_2](ClO_4)_2$ (**4**), $[Zn(Ph\text{-}tpy)_2](ClO_4)_2$ (**5**) and $[Zn(Fc\text{-}dpa)_2](PF_6)_2$ (**6a**) were grown by the diffusion method by layering diethyl ether onto the MeCN or MeOH solution of the complexes. Crystal mounting was done on glass fibre using epoxy glue. Data collection for the complexes were done at 293 K using a diffractometer (Bruker Smart Kappa APEX II CCD Detector) with a fine-focused sealed tube with graphite-monochromated Mo-Kα radiation (λ = 0.71073 Å) using ω-scan mode. The molecular structures of the complexes were solved by direct methods and refinement was done by full-matrix least squares based on F^2 using SHELX-97 program.[61] Empirical absorption corrections were made by using multi-scan program.[62] All non-hydrogen atoms were refined anisotropically, while the hydrogen atoms were typically placed in their calculated positions and constrained to a riding model. The perspective views of the complexes were obtained using ORTEP-3 for Windows.[63] Selected crystallographic data are given in Table 5.

DNA binding and cleavage experiments

The DNA binding and cleavage experiments were carried out using calf thymus DNA and SC pUC19 DNA by following literature

Table 5 Selected crystallographic data for the complexes **2**·MeOH.MeCN, **4**·2MeCN, **5** and **6a**

	2·MeOH.MeCN	**4**·2MeCN	**5**	**6a**
Empirical formula	$C_{54}H_{45}Cl_2CoFe_2N_7O_9$	$C_{54}H_{44}Cl_2Fe_2N_8O_8Zn$	$C_{42}H_{30}Cl_2N_6O_8Zn$	$C_{46}H_{46}F_{12}Fe_2N_6P_2Zn$
Fw / g M^{-1}	1177.50	1180.94	882.99	1149.90
Crystal system	Monoclinic	Monoclinic	Monoclinic	Orthorhombic
Space group	$C2/c$	$C2/c$	$P2_1/c$	$Pbcn$
a/Å	20.8487(12)	20.804(2)	9.5145(3)	21.776(2)
b/Å	19.1791(11)	19.191(2)	12.8131(5)	11.5108(11)
c/Å	12.9275(7)	13.0849912)	31.5604(12)	19.0161(18)
β/°	96.567(3)	96.236(8)	97.368(2)	90.00
U/Å^3	5135.3(5)	5193.2(9)	3815.8(2)	4766.47(8)
Z	4	4	4	4
$2\theta_{max}$ (°)	56.00	52.00	51.00	56.70
T/K	293(2)	293(2)	293(2)	293
ρ_c/g cm^{-3}	1.523	1.510	1.537	1.602
λ/Å (Mo-Kα)	0.71073	0.71073	0.71073	0.71073
μ/mm^{-1}	1.046	1.175	0.849	1.255
Data / restraints / parameters	6212 / 0 / 345	5093 / 0 / 350	11354 / 0 / 532	5798 / 0 / 305
F(000)	2412	2416	1676	2336
Goodness-of-fit	1.007	1.012	1.064	1.021
R (F_o)[a], $I > 2\sigma(I)$ [wR (F_o)[b]]	0.0659[0.1699]	0.0843 [0.2303]	0.0642[0.1766]	0.0716[0.1700]
R (all data) [wR (all data)]	0.1600[0.2174]	0.1662 [0.2813]	0.1007[0.2005]	0.1420[0.2071]
Largest diff. peak and hole/e Å^{-3}	0.961, –0.707	0.961, –0.410	1.548, –0.557	0.852, –0.717
$w = 1 / [\sigma^2(F_o^2) + (AP)^2 + (BP)]$	A = 0.1044	A = 0.1572	A = 0.1057	A = 0.0952
	B = 2.3929	B = 0.0000	B = 4.4709	B = 6.2663

[a] $R = \Sigma \mid F_o \mid - \mid F_c \mid / \Sigma \mid F_o \mid$. [b] $wR = \{\Sigma[w(F_o^2 - F_c^2)^2] / \Sigma[w(F_o)^2]\}^{1/2}$; $w = [\sigma^2(F_o)^2 + (AP)^2 + BP]^{-1}$, where $P = (F_o^2 + 2F_c^2)/3$.

procedures (see ESI† for details).[37,64] For UV-visible absorption titration, Tris-HCl buffer of pH 7.2 was used and the concentration of calf thymus DNA and complex were 150 μM and 15–25 μM, respectively. DNA thermal denaturation experiments were carried out in phosphate buffer (pH 6.8) by varying the temperature from 40 °C to 90 °C. The ratio of the complex and DNA concentration was 1 : 10. The DNA viscometric titrations were carried out in Tris-HCl buffer (pH 7.2). The SC pUC19 DNA cleavage activity of the complexes (**1–6**) was studied in visible light of 532 nm and 647 nm using a CW (continuous wave) Ar-Kr mixed gas ion laser (Spectra Physics Water-Cooled Mixed-Gas Ion Laser Stabilite® 2018-RM) or in the dark using external additives like glutathione (GSH) and hydrogen peroxide. For DNA photocleavage mechanistic studies, singlet oxygen quenchers and radical scavengers were used to detect the ROS. Photolysis experiments were carried out in aqueous DMF or MeCN using UV-A light of 365 nm.

Cell culture

HeLa (human cervical carcinoma) cells were maintained in Dulbecco's Modified Eagle's Medium (DMEM), supplemented with 10% fetal bovine serum (FBS), 100 IU ml^{-1} of penicillin, 100 μg ml^{-1} of streptomycin and 2 mM Glutamax at 37 °C in a humidified incubator at 5% CO_2. The adherent cultures were grown as monolayer and were passaged once in 4–5 days by trypsinizing with 0.25% Trypsin-EDTA.

Photocytotoxicity experiments

Cytotoxicity measurements of the complexes **1–6** in dark or light were carried out from the MTT assay which is based on the cleavage of tetrazolium rings of MTT by mitochondrial dehydrogenases in the viable cells to formazan, a dark blue membrane impermeable species that can be quantified at 540 nm on solubilisation in DMSO solution giving a measure of the number of viable cells.[65] Approximately, 10^4 HeLa cells in a 96-well culture plate in DMEM containing 10% FBS were incubated for 24 h at 37 °C in a CO_2 incubator, followed by the addition of the complex solution in a medium containing 1% DMSO. After 4 h incubation in the dark, the medium was replaced by fresh phosphate buffered saline (PBS) and the culture plate was placed inside the Luzchem Photoreactor (Model LZC-1, Ontario, Canada) fitted with Sylvania make 8 fluorescent white tubes with a fluence rate of 2.4 mW cm^{-2} to provide a total dose of 10 J cm^{-2} for photoexposure to 400–700 nm visible light. After 1 h of photoirradiation, PBS was replaced by fresh medium, and further incubated for 24 h in the dark. Finally, 25 μL of 4 mg ml^{-1} MTT was added to each well and again incubated for an additional 3 h. After discarding the culture medium, 200 μL of DMSO was added to dissolve the formazan crystals formed, and the absorbance at 540 nm was measured using a BIORAD ELISA plate reader. The cytotoxicity was measured from the absorbance ratio of the treated cells and untreated controls. Each experiment was conducted with samples in triplicate and the data given were based on three experimental values.

FACScan analysis

HeLa cells (0.5×10^6 cells) plated overnight were treated with different concentrations of complex **4** in DMEM for 4 h, followed by exposure to visible light for 1 h. The cells were then cultured overnight, harvested and fixed using chilled 70% ethanol. The cells were then treated with 50 μg ml^{-1} RNase A overnight and stained with propidium iodide (PI) staining solution (20 μg ml^{-1} PI in PBS) for 2 h at 4 °C. The cells were analyzed using flow cytometry (FACSCanto, Beckton Dickenson) to determine the % apoptotic population.[66]

Acknowledgements

We thank the Department of Science and Technology (DST), Government of India, for financial support (SR/S5/MBD-02/2007). We are thankful to DST for a CCD diffractometer facility, Alexander Von Humboldt Foundation, Germany, for donation of an electroanalytical system, and Dr O. Joy, P. Pai and Kavya A. of the FACS facility funded by the Department of Biotechnology, Government of India. A. R. C. thanks the DST for a J. C. Bose national fellowship. SG and TKG thank CSIR, New Delhi, for research fellowships.

References

1 Y. Jung and S. J. Lippard, *Chem. Rev.*, 2007, **107**, 1387.
2 Z. Guo and P. J. Sadler, *Angew. Chem., Int. Ed.*, 1999, **38**, 1512.
3 S. P. Fricker, *Dalton Trans.*, 2007, 4903.
4 C. G. Hartinger and P. J. Dyson, *Chem. Soc. Rev.*, 2009, **38**, 391.
5 U. Schatzschneider, *Eur. J. Inorg. Chem.*, 2010, 1451.
6 N. L. Fry and P. K. Mascharak, *Acc. Chem. Res.*, 2011, **44**, 289.
7 N. J. Farrer, L. Salassa and P. J. Sadler, *Dalton Trans.*, 2009, 10690.
8 H. T. Chifotides and K. R. Dunbar, *Acc. Chem. Res.*, 2005, **38**, 146.
9 L. J. K. Boerner and J. M. Zaleski, *Curr. Opin. Chem. Biol.*, 2005, **9**, 135.
10 D. Crespy, K. Landfester, U. S. Schubert and A. Schiller, *Chem. Commun.*, 2010, **46**, 6651.
11 S. Dhar, Z. Liu, Z. J. Thomale, H. Dai and S. J. Lippard, *J. Am. Chem. Soc.*, 2008, **130**, 11467.
12 S. Dhar and S. J. Lippard, *Proc. Natl. Acad. Sci. U. S. A.*, 2009, **106**, 22199.
13 A. S. Paraskar, S. Soni, K. T. Chin, P. Chaudhuri, K. W. Muto, J. Berkowitz, M. W. Handlogten, N. J. Alves, B. Bilgicer, D. M. Dinulescu, R. A. Mashelkar and S. Sengupta, *Proc. Natl. Acad. Sci. U. S. A.*, 2010, **107**, 12435.
14 Z. Ma, J. Roy Choudhury, M. W. Wright, C. S. Day, G. Saluta, G. L. Kucera and U. Bierbach, *J. Med. Chem.*, 2008, **51**, 7574.
15 F. S. Mackay, J. A. Woods, P. Heringová, J. Kašpárková, A. M. Pizarro, S. A. Moggach, S. Parsons, V. Brabec and P. J. Sadler, *Proc. Natl. Acad. Sci. U. S. A.*, 2007, **104**, 20743.
16 R. Bonnett, *Chemical Aspects of Photodynamic Therapy*Gordon & Breach: London, U.K., 2000.
17 J. P. Celli, B. Q. Spring, I. Rizvi, C. L. Evans, K. S. Samkoe, S. Verma, B. W. Pogue and T. Hasan, *Chem. Rev.*, 2010, **110**, 2795.
18 M. Ethirajan, Y. Chen, P. Joshi and R. K. Pandey, *Chem. Soc. Rev.*, 2011, **40**, 340.
19 B. W. Henderson, T. M. Busch, L. A. Vaughan, N. P. Frawley, D. Babich, T. A. Sosa, J. D. Zollo, A. S. Dee, M. T. Cooper, D. A. Bellnier, W. R. Greco and A. R. Oseroff, *Cancer Res.*, 2000, **60**, 525.
20 M. Ochsner, *J. Photochem. Photobiol., B*, 1996, **32**, 3.
21 S. I. Moriwaki, J. Misawa, Y. Yoshinari, I. Yamada, M. Takigawa and Y. Tokura, *Photodermatol., Photoimmunol. Photomed.*, 2001, **17**, 241.
22 C. J. Burrows and J. G. Muller, *Chem. Rev.*, 1998, **98**, 1109.
23 K. Szacilowski, W. Macyk, A. Drzewiecka-Matuszek, M. Brindell and G. Stochel, *Chem. Rev.*, 2005, **105**, 2647.
24 A. M. Angeles-Boza, H. T. Chifotides, J. D. Aguirre, A. Chouai, P. K.-L. Fu, K. R. Dunbar and C. Turro, *J. Med. Chem.*, 2006, **49**, 6841.
25 S. Saha, R. Majumdar, M. Roy, R. R. Dighe and A. R. Chakravarty, *Inorg. Chem.*, 2009, **48**, 2652.
26 P. K. Sasmal, S. Saha, R. Majumdar, R. R. Dighe and A. R. Chakravarty, *Chem. Commun.*, 2009, 1703.
27 A. A. Holder, D. F. Zigler, M. T. Tarrago-Trani, B. Storrie and K. J. Brewer, *Inorg. Chem.*, 2007, **46**, 4760.
28 A. D. Ostrowski and P. C. Ford, *Dalton Trans.*, 2009, 10660.
29 M. J. Rose, N. L. Fry, R. Marlow, L. Hinck and P. K. Mascharak, *J. Am. Chem. Soc.*, 2008, **130**, 8834.
30 M. Brindell, E. Kulís, S. K. Elmroth, K. Urbánska and G. Stochel, *J. Med. Chem.*, 2005, **48**, 7298.
31 D. R. Van Staveren and N. Metzler-Nolte, *Chem. Rev.*, 2004, **104**, 5931.
32 G. Jaouen, S. Top, A. Vessires, G. Leclercq and M. J. McGlinchey, *Curr. Med. Chem.*, 2004, **11**, 2505.
33 W. Daher, C. Biot, T. Fandeur, H. Jouin, L. Pelinski, E. Viscogliosi, L. Fraisse, B. Pradines, J. Brocard, J. Khalife and D. Dive, *Malar. J.*, 2006, **5**, 11.
34 G. Tabbì, C. Cassino, G. Cavigiolio, D. Colangelo, A. Ghiglia, I. Viano and D. Osella, *J. Med. Chem.*, 2002, **45**, 5786.
35 M. F. R. Fouda, M. M. Abd-Elzaher, R. A. Abdelsamaia and A. A. Labib, *Appl. Organomet. Chem.*, 2007, **21**, 613.
36 G. Gasser, I. Ott and N. Metzler-Nolte, *J. Med. Chem.*, 2011, **54**, 3.
37 B. Maity, M. Roy, B. Banik, R. Majumdar, R. R. Dighe and A. R. Chakravarty, *Organometallics*, 2010, **29**, 3632.
38 S. Ramakrishnan, V. Rajendiran, M. Palaniandavar, V. S. Periasamy, B. S. Srinag, H. Krishnamurthy and M. A. Akbarsha, *Inorg. Chem.*, 2009, **48**, 1309.
39 P. U. Maheswari, M. van der Ster, S. Smulders, S. Barends, G. P. van Wezel, C. Massera, S. Roy, H. den Dulk, P. Gamez and J. Reedijk, *Inorg. Chem.*, 2008, **47**, 3719.
40 K. Hutchison, J. C. Morris, T. A. Nile, J. L. Walsh, D. W. Thompson, J. D. Petersen and J. R. Schoonover, *Inorg. Chem.*, 1999, **38**, 2516.
41 U. Siemeling, J. Vor der Brüggen, U. Vorfeld, B. Neumann, A. Stammler, H.-G. Stammler, A. Brockhinke, R. Plessow, P. Zanello, F. Laschi, F. F. de Biani, M. Fontani, S. Steenken, M. Stapper and G. Gurzadyan, *Chem.–Eur. J.*, 2003, **9**, 2819.
42 J. Gleru, P. A. Coodson, D. J. Hodgson, K. Michelsen, K. M. Nielsen and H. Wehe, *Inorg. Chem.*, 1992, **31**, 4611.
43 J. McMurtrie and I. Dance, *CrystEngComm*, 2009, **11**, 1141.
44 R. Indumathy, S. Radhika, M. Kanthimathi, T. Weyhermuller and B. U. Nair, *J. Inorg. Biochem.*, 2007, **101**, 434.
45 A. M. Pyle, J. P. Rehmann, R. Meshoyrer, C. V. Kumar, N. J. Turro and J. K. Barton, *J. Am. Chem. Soc.*, 1989, **111**, 3051.
46 J. M. Kelly, A. B. Tossi, D. J. McConnell and C. OhUigin, *Nucleic Acids Res.*, 1985, **13**, 6017.
47 J. M. Veal and R. L. Rill, *Biochemistry*, 1991, **30**, 1132.
48 T. A. Van den Berg, B. L. Feringa and G. Roelfes, *Chem. Commun.*, 2007, 180.
49 S. Dhar, P. A. N. Reddy and A. R. Chakravarty, *Dalton Trans.*, 2004, 697.
50 K. E. Erkkila, D. T. Odom and J. K. Barton, *Chem. Rev.*, 1999, **99**, 2777.
51 S. Roy, S. Saha, R. Majumdar, R. R. Dighe and A. R. Chakravarty, *Polyhedron*, 2010, **29**, 3251.
52 E. Delaey, F. van Laar, D. De Vos, A. Kamuhabwa, P. Jacobs and P. de Witte, *J. Photochem. Photobiol., B*, 2000, **55**, 27.
53 H. C. Kang, I.-J. Kim, H.-W. Park, S.-G. Jang, S.-A. Ahn, S. N. Yoon, H.-J. Chang, B. C. Yoo and J.-G. Park, *Cancer Lett.*, 2007, **247**, 40.
54 S. Saha, D. Mallick, R. Majumdar, M. Roy, R. R. Dighe, E. D. Jemmis and A. R. Chakravarty, *Inorg. Chem.*, 2011, **50**, 2975.
55 D. D. Perrin, W. L. F. Armarego, D. R. Perrin, *Purification of Laboratory Chemicals*, Pergamon Press, Oxford, 1980.
56 E. C. Constable, A. J. Edwards, R. Martínez-Máñez, P. R. Raithby and A. M. W. C. Thompson, *J. Chem. Soc., Dalton Trans.*, 1994, 645.
57 S. A. Moya, R. Pastene, H. L. Bozec, P. J. Baricelli, A. J. Pardey and J. Gimeno, *Inorg. Chim. Acta*, 2001, **312**, 7.
58 E. C. Constable, J. Lewis, M. C. Liptrot and P. R. Raithby, *Inorg. Chim. Acta*, 1990, **178**, 47.
59 A. J. Evans, S. E. Watkins, D. C. Craig and S. B. Colbran, *J. Chem. Soc., Dalton Trans.*, 2002, 983.
60 D. F. Evans and T. A. James, *J. Chem. Soc., Dalton Trans.*, 1979, 723.
61 G. M. Sheldrick, *Acta Crystallogr., Sect. A: Found. Crystallogr.*, 2008, **A64**, 112.
62 N. Walker and D. Stuart, *Acta Crystallogr., Sect. A: Found. Crystallogr.*, 1983, **A39**, 158.
63 C. K. Johnson, *ORTEP-III, Report ORNL-5138*Oak Ridge National Laboratory: Oak Ridge, TN, 1976.
64 S. Dhar, M. Nethaji and A. R. Chakravarty, *Inorg. Chem.*, 2005, **44**, 8876.
65 T. Mosmann, *J. Immunol. Methods*, 1983, **65**, 55.
66 X. Qu and L. Qing, *J. Biochem. Mol. Biol.*, 2004, **37**, 445.